

# STM/STS Investigations of Topological Surface States on Sb Thin Films

- Guanggeng YAO<sup>1</sup>, Feng PAN<sup>1</sup>, Jiatao SUN<sup>2</sup>, Wentao XU<sup>1</sup>, Xinjun CHU<sup>1</sup>, Ziyu LUO<sup>1</sup>, Wei CHEN<sup>2</sup>, Andrew WEE<sup>1</sup>, Xue-Sen WANG<sup>1\*</sup>
- <sup>1</sup>Department of Physics, National University of Singapore,
- <sup>2</sup>Department of Chemistry, National University of Singapore

## [Introduction]

Antimony (Sb) is a semimetal with a negative indirect gap. But it possesses novel topologically protected electronic surface states (SSs) similar to a topological insulator (TI). So far, the reported experimental studies using angle-resolved photoemission spectroscopy (ARPES) and scanning tunneling microscopy/spectroscopy (STM/STS) have been performed only on bulk-cleaved Sb(111) samples. Here, we have grown Sb(111) thin films on Si(111)- $\sqrt{3}\times\sqrt{3}$ :Bi- $\beta$  in ultra-high vacuum, and characterized them with in situ STM/STS to verify the robust spin-polarized Dirac fermions on Sb(111) surfaces. Our studies show that flat and well-ordered Sb thin films following the Frank-Van der Merwe mode are achievable whose topological SSs can be detected. Additionally, by Fourier transform of STM  $dI/dV$  maps (FT-STS) to obtain k-space information, characteristic distributions of the scattering channels along high-symmetry directions on the surface change dramatically with the thickness of Sb(111) films due to the quantum confinement effect (QCE). The Sb(111) thin films as an elemental TI should offer certain advantages over compound and alloy TIs that are essential to applications, such as low bulk and surface defect densities.

## [Experiment]

- Experiments were carried out in the Unisoku UHV LT-STM System with the base pressure better than  $1 \times 10^{-10}$  mbar.
- Si was degassed at 600 °C for several hours, followed by stepwise heating up to 900 °C and then by rapid flashing at 1200 °C.
- To obtain Si(111)- $\sqrt{3}\times\sqrt{3}$ :Bi- $\beta$  surface reconstruction, 2ML Bi is deposited on Si(111)- $7\times 7$  at room temperature and afterwards annealed at about 450°C to obtain a trimer reconstruction.
- High purity Sb evaporated from the crucible at 400°C.
- STM/STS were taken at 4.2K (liquid helium temperature). The  $dI/dV$  spectrum was acquired using a lock-in amplifier with the bias voltage modulated at a frequency of 800 Hz and peak-to-peak amplitude of 5 mV.

## [Result and Discussion]

### 1. Schematic structure and STM/STS of Sb

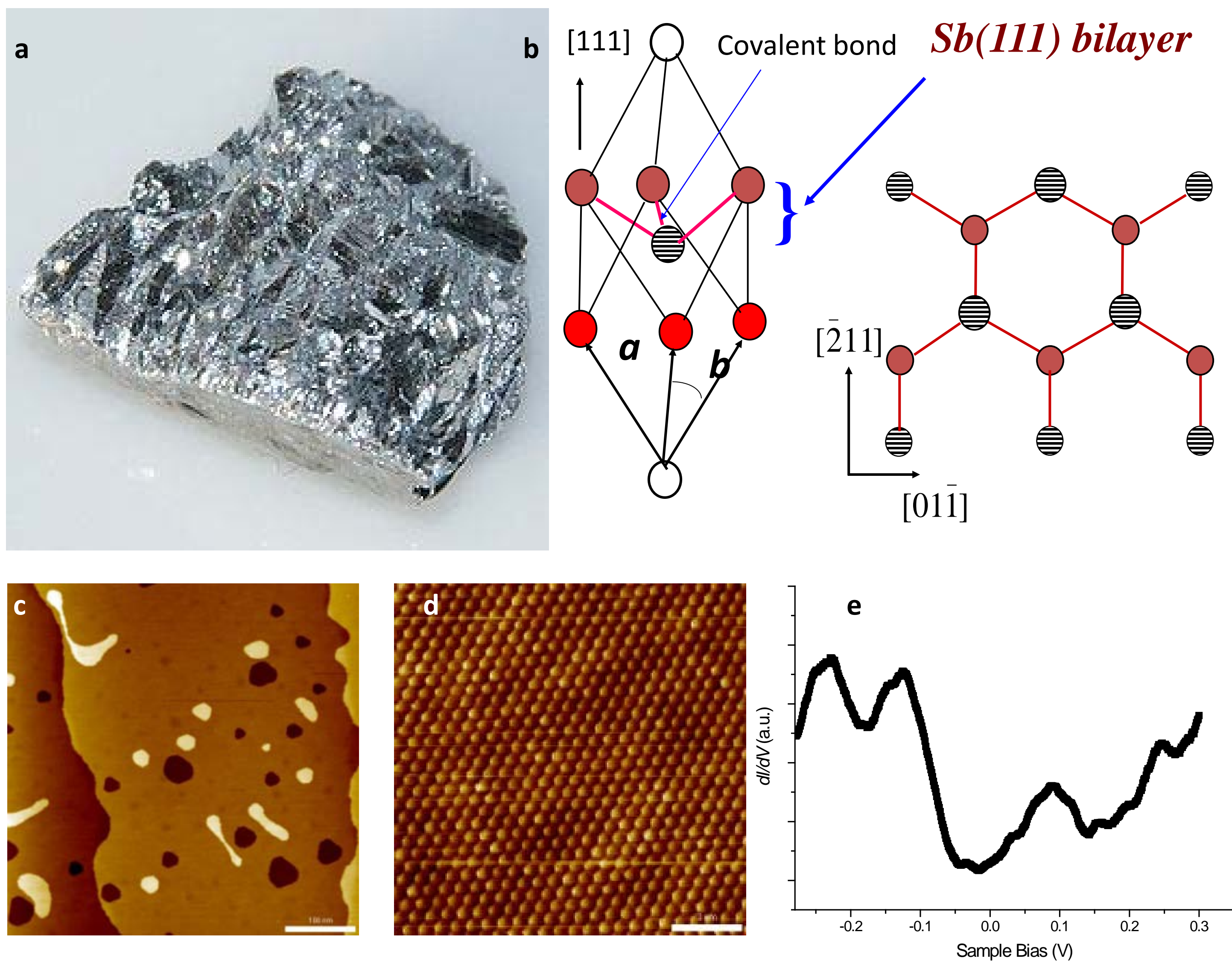


Fig. 1 (a) Bulk Sb crystal. (b) Schematics of rhombohedral lattice for Sb. The left one shows the unit cell. The right one viewed in [111] trigonal direction with in-plane atomic period of 4.31 Å. (c) The STM topography of Sb(111) film. Imaging condition: V=2V, I=50pA. (d) The atomic-resolution image on the bare surface. Imaging condition: V=0.5V, I=100pA. (e)  $dI/dV$  spectrum

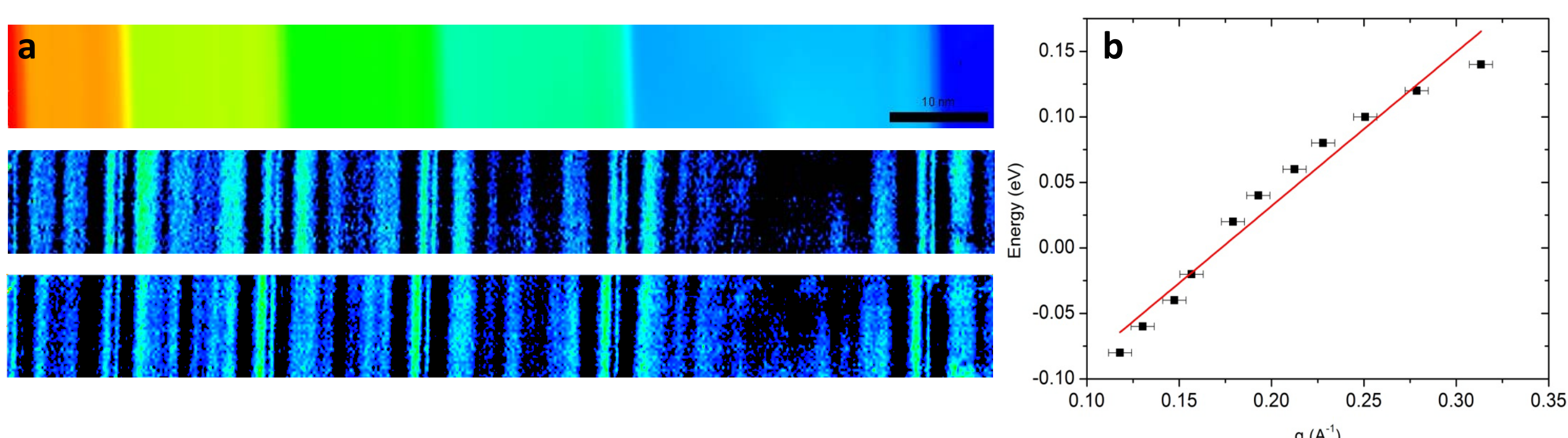


Fig. 2 (a) Upper one: The STM topography of multiple steps on Sb (~30BL). Lower two: representative  $dI/dV$  mapping at the upper location using bias at 160mV and 140mV, respectively. (b) Energy dispersion as a function of k derived from a series of  $dI/dV$  mapping. The fitting slope here is 1.18 eVÅ, which is in excellent agreement with ARPES measurements (1.2 eVÅ).<sup>1</sup> Here the error bar corresponds to  $2\pi/1000$  Å.<sup>2</sup>

### 3. Spatially- and energetically-resolved $dI/dV$ measurements

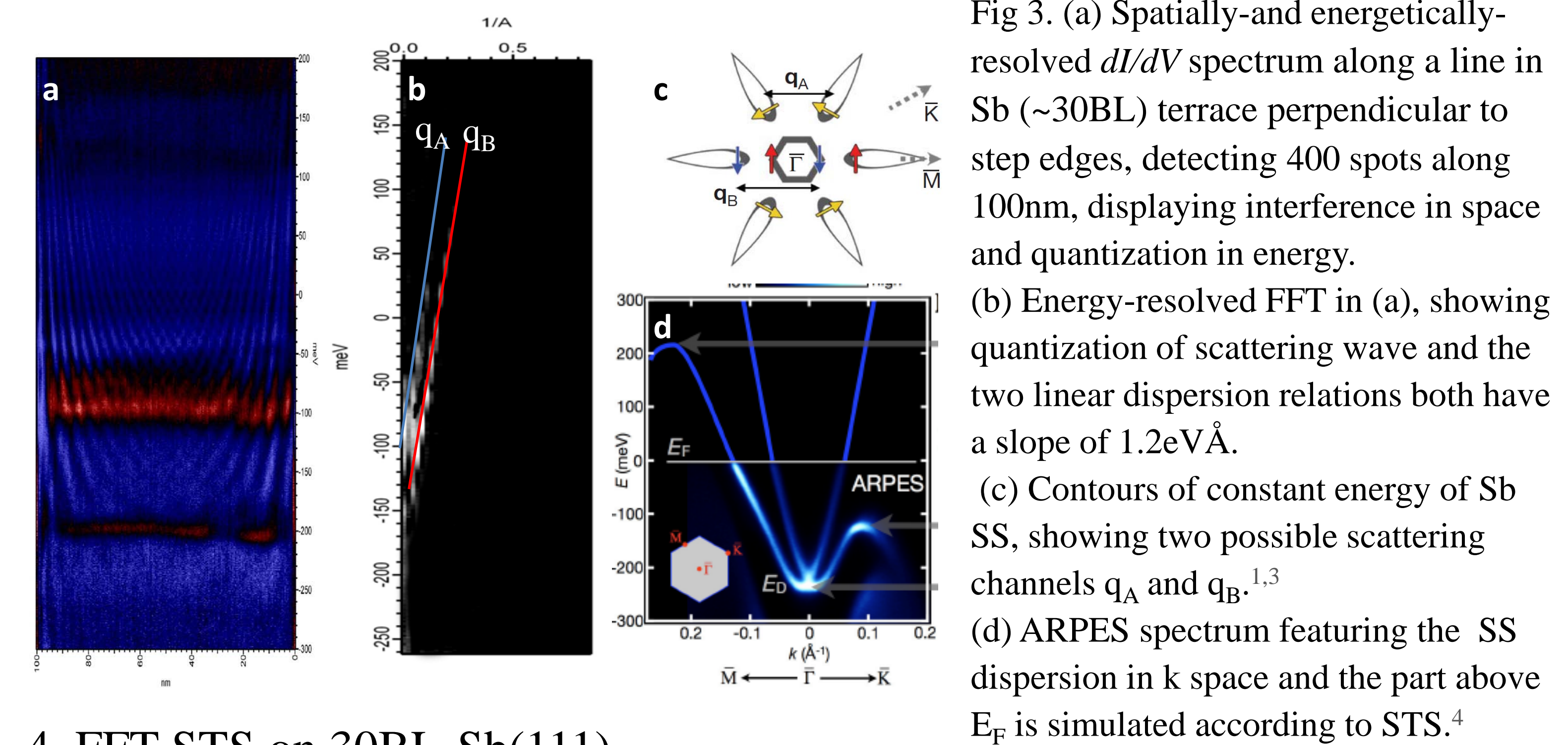


Fig 3. (a) Spatially- and energetically-resolved  $dI/dV$  spectrum along a line in Sb (~30BL) terrace perpendicular to step edges, detecting 400 spots along 100nm, displaying interference in space and quantization in energy. (b) Energy-resolved FFT in (a), showing quantization of scattering wave and the two linear dispersion relations both have a slope of 1.2eVÅ. (c) Contours of constant energy of Sb SS, showing two possible scattering channels  $q_A$  and  $q_B$ .<sup>1,3</sup> (d) ARPES spectrum featuring the SS dispersion in k space and the part above  $E_F$  is simulated according to STS.<sup>4</sup>

### 4. FFT-STS on 30BL-Sb(111)

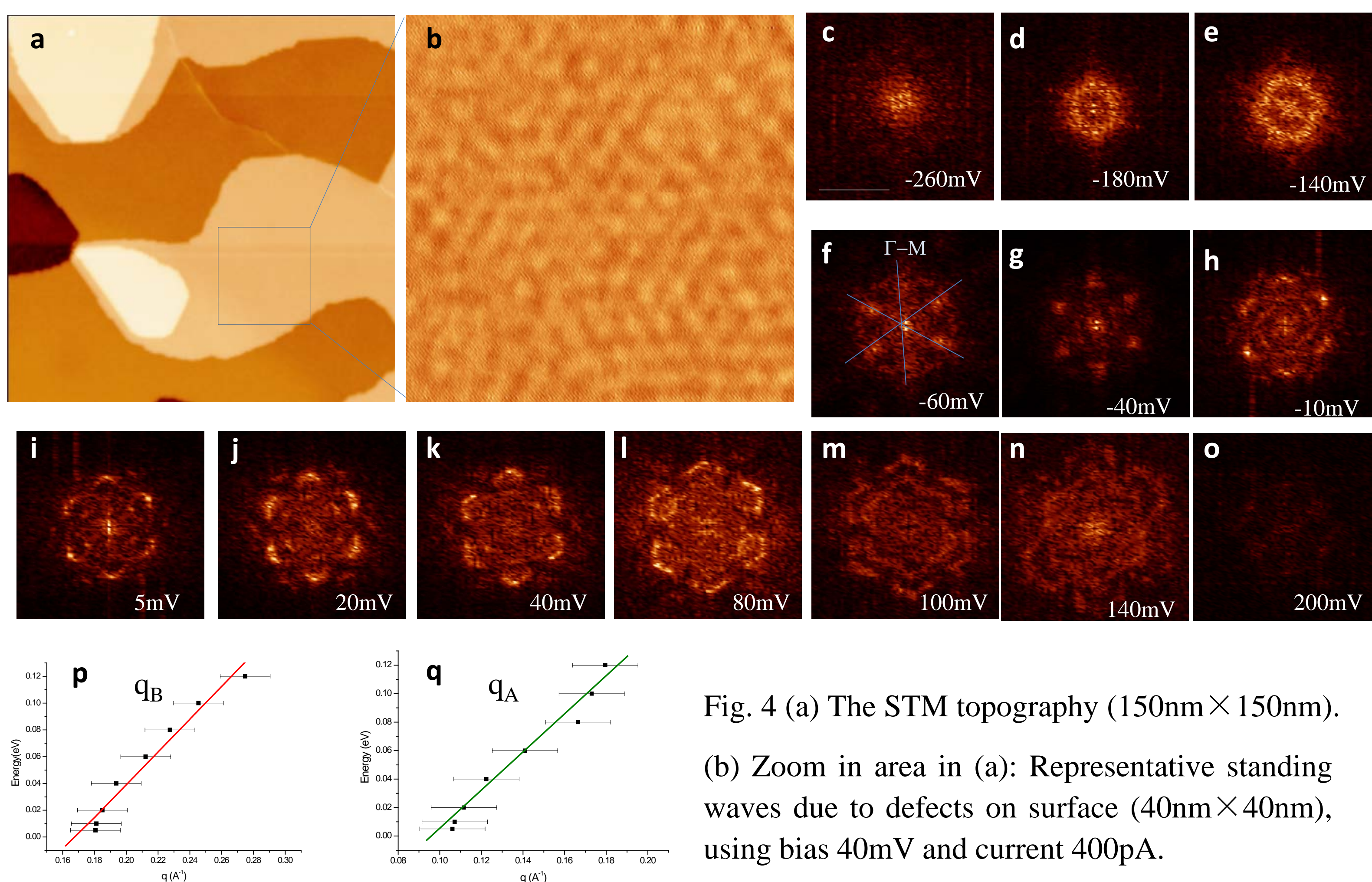


Fig. 4 (a) The STM topography (150nm  $\times$  150nm). (b) Zoom in area in (a): Representative standing waves due to defects on surface (40nm  $\times$  40nm), using bias 40mV and current 400pA. (c-o) FFT-STS performed at same area in (b). Scale bar in (c):  $0.5 \text{ nm}^{-1}$ . Fig. (c) to (o) are of the same size and orientation, following the one marked in (f).  $\Gamma$ -M is the prominent scattering direction as previously reported<sup>3</sup>. (p-q) Energy dispersion relationship by analyzing k peaks along  $\Gamma$ -M. Data in (p-q) are selected from outer and inner k peaks in FFT-STS, corresponding to  $q_B$  and  $q_A$ , respectively. The slopes in (p-q) are 1.22 and 1.29 eVÅ, which are comparable with Fig. 3(b). The error bar corresponds to  $2\pi/400$  Å.

### 5. FFT-STS on 9BL-Sb(111)

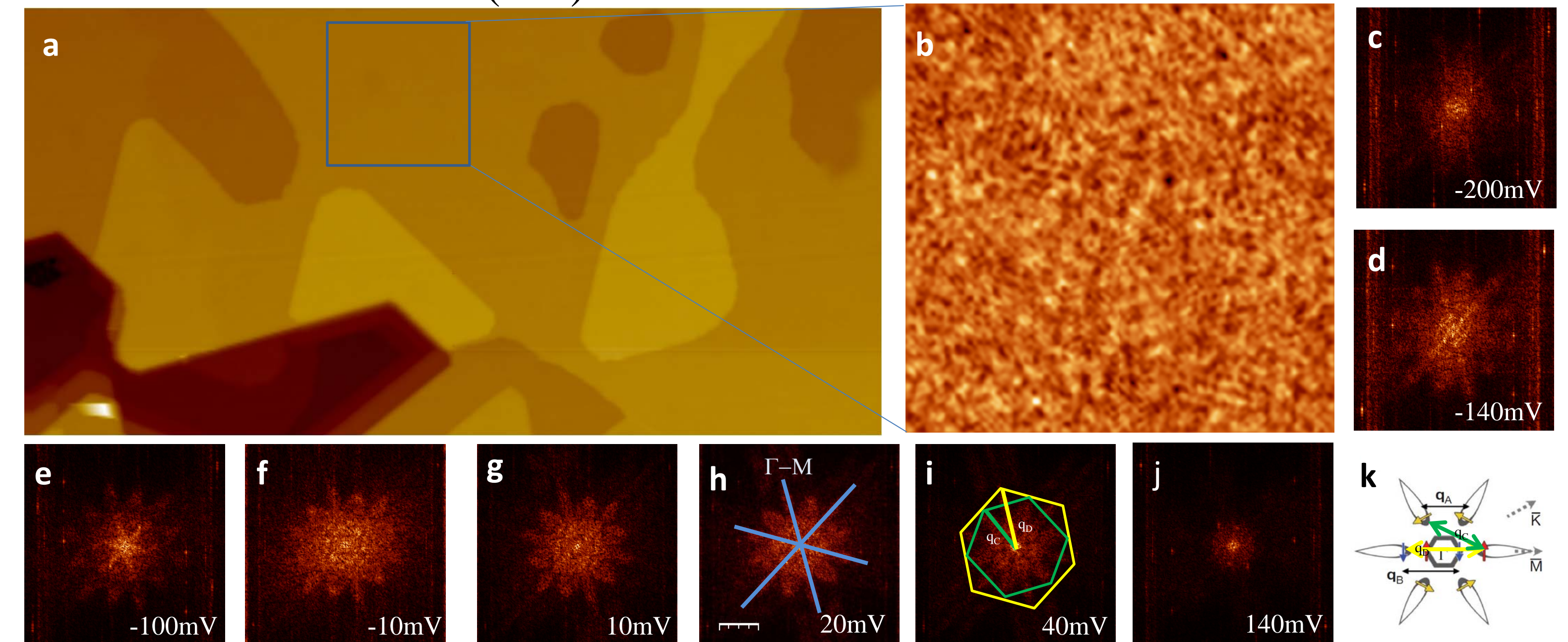


Fig. 5 (a) The STM topography (300nm  $\times$  150nm). (b) Zoom in area in (a): Representative standing waves (50nm  $\times$  50nm), using bias 20mV and current 120pA. (c-j) FFT-STS performed at same area in (b). Scale bar in (h):  $0.62 \text{ nm}^{-1}$ . Fig. (c) to (j) are of the same size and orientation, following the one marked in (h). Different from 30BL case, here both  $\Gamma$ -M and  $\Gamma$ -K are the prominent scattering directions. The reason is when the film is thin enough, the coupling of two SSs can break the TRS and open up new scattering channels. (i) and (k) show the origin of the two dominate directions coming from  $q_C$  (marked as green line) and  $q_D$  (marked as yellow line). And the scale of  $q_C$  and  $q_D$  in (i) illustrates excellent agreement with (k), demonstrating a reasonable ratio of  $\sqrt{3}/2$ .

## [Conclusion]

In this work, we fabricated Sb(111) thin films with different thickness successfully, and investigated the SSs by STS measurements. Explicit changes in the surface scattering phenomena can be observed when the thickness is changed, due to the presence or absence of SSs coupling. This offers a great opportunity to facilitate applications of TI in spintronics and topological quantum computation by tuning the thickness.<sup>5</sup>

- Seo, J., P. Roushan, et al. (2010). *Nature* **466**: 343
- Zhang, T., P. Cheng, et al. (2009) *Physical Review Letters* **103**: 266803
- Hsieh, D, et al. (2009). *Science* **323**: 919
- [arXiv:0909.0921v2](https://arxiv.org/abs/0909.0921v2) [cond-mat.mes-hall]
- He, K, et al. (2010) *Nat Phys* **6**: 584